Article

Molecular Cell

High-Affinity Sites Form an Interaction Network to Facilitate Spreading of the MSL Complex across the X Chromosome in *Drosophila*

Graphical Abstract

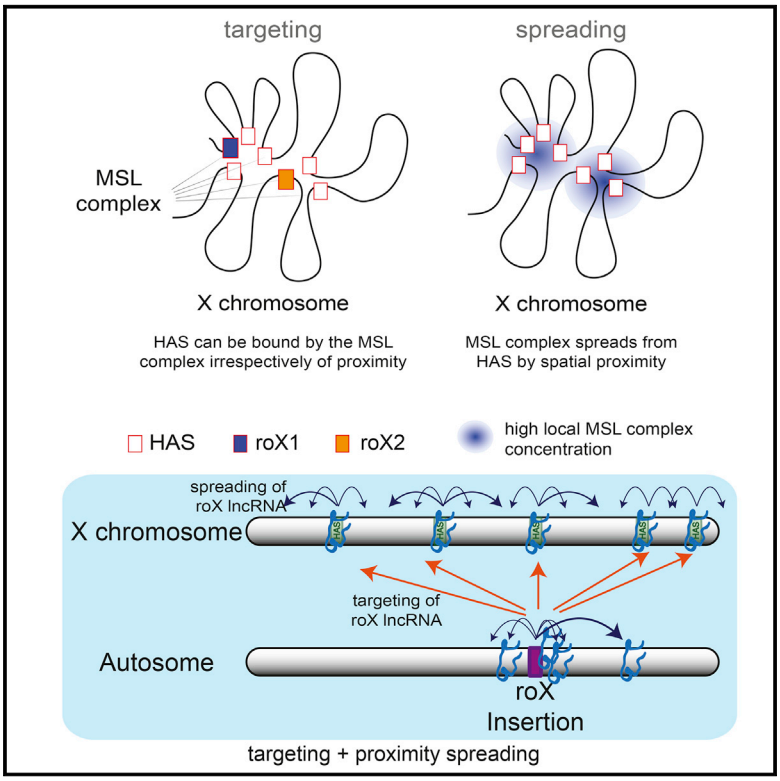

Authors

Fidel Ramírez, Thomas Lingg, Sarah Toscano, ..., Job Dekker, Thomas Manke, Asifa Akhtar

Correspondence

akhtar@ie-freiburg.mpg.de

In Brief

Combining chromosome conformation analyses with fly genetics, Ramírez et al. show that high-affinity sites (HAS), positioned at hubs of long-range chromatin contacts, arrange in a sex- and MSL complex-independent manner on the X chromosome. The MSL complex spreads via spatial proximity and regulates local chromatin remodeling rather than influencing global chromatin architecture.

Highlights

- HAS frequently occur at regions with enriched long-range contacts on the X chromosome
- Global X chromosome architecture is sex- and MSL complex-independent in flies
- roX HAS dynamically organize within the X territory depending on transcriptional status
- The MSL complex uses spatial proximity to spread and affects nucleosome pattern at HAS

Accession Numbers

GSE58821

Ramírez et al., 2015, Molecular Cell *60*, 146–162
October 1, 2015
http://dx.doi.org/10.1016/j.molcel.2015.08.024

CellPress

Molecular Cell
Article

High-Affinity Sites Form an Interaction Network to Facilitate Spreading of the MSL Complex across the X Chromosome in *Drosophila*

Fidel Ramírez,[1,7] Thomas Lingg,[1,2,7] Sarah Toscano,[1,7] Kin Chung Lam,[1,2,7] Plamen Georgiev,[1] Ho-Ryun Chung,[3] Bryan R. Lajoie,[4] Elzo de Wit,[5] Ye Zhan,[4] Wouter de Laat,[5] Job Dekker,[4,6] Thomas Manke,[1] and Asifa Akhtar[1,*]

[1]Max Planck Institute of Immunobiology and Epigenetics, 79108 Freiburg, Germany
[2]Faculty of Biology, University of Freiburg, 79104 Freiburg, Germany
[3]Max Planck Institute for Molecular Genetics, 14195 Berlin, Germany
[4]Program in Systems Biology, Department of Biochemistry and Molecular Pharmacology, University of Massachusetts Medical School, Worcester, MA 01605-0103, USA
[5]Hubrecht Institute, Royal Netherlands Academy of Arts and Sciences and University Medical Center Utrecht, Uppsalalaan 8, 3584 CT Utrecht, the Netherlands
[6]Howard Hughes Medical Institute
[7]Co-first author
*Correspondence: akhtar@ie-freiburg.mpg.de
http://dx.doi.org/10.1016/j.molcel.2015.08.024

SUMMARY

Dosage compensation mechanisms provide a paradigm to study the contribution of chromosomal conformation toward targeting and spreading of epigenetic regulators over a specific chromosome. By using Hi-C and 4C analyses, we show that high-affinity sites (HAS), landing platforms of the male-specific lethal (MSL) complex, are enriched around topologically associating domain (TAD) boundaries on the X chromosome and harbor more long-range contacts in a sex-independent manner. Ectopically expressed roX1 and roX2 RNAs target HAS on the X chromosome in *trans* and, via spatial proximity, induce spreading of the MSL complex in *cis*, leading to increased expression of neighboring autosomal genes. We show that the MSL complex regulates nucleosome positioning at HAS, therefore acting locally rather than influencing the overall chromosomal architecture. We propose that the sex-independent, three-dimensional conformation of the X chromosome poises it for exploitation by the MSL complex, thereby facilitating spreading in males.

INTRODUCTION

The organization of chromosomes within the nucleus and the spatial arrangement of genes within a chromosome territory are gaining fundamental importance during epigenetic control of gene expression (Quinodoz and Guttman, 2014). Notably, the regulatory mechanisms of sex chromosomes offer ideal paradigms to understand how the expression of an entire chromosome, and, therefore, thousands of genes at once, can be controlled by epigenetic mechanisms (Brockdorff and Turner, 2015).

Dimorphic sex chromosomes genetically determine sex in many organisms. In the XX/XY sex determination system, males are heterogametic (XY), and females are homogametic (XX). To overcome the risk of an unequal transcriptional output, different organisms have evolved independent strategies (termed "dosage compensation") to balance the X chromosomal gene dose between the sexes (Vicoso and Charlesworth, 2006). In mammals, expression of the long non-coding RNA (lncRNA) Xist from only one of the two female X chromosomes leads to recruitment of silencing complexes in *cis* through which this chromosome becomes compacted and heterochromatinized (Heard and Disteche, 2006). In *Drosophila melanogaster*, dosage compensation happens on the single male X chromosome by formation of the male-specific lethal (MSL) complex, which promotes an approximately 2-fold transcriptional upregulation (Conrad and Akhtar, 2011). The MSL complex consists of four core proteins (MSL1, MSL2, MSL3, and males absent on the first [MOF]) which, together, form a hetero-octameric complex that is further stabilized by the integration of two lncRNAs, called RNA on the X chromosome (roX) 1 and 2, by the ATP-dependent RNA helicase maleless (MLE) (Keller and Akhtar, 2015). The formation of this ribonucleoprotein complex is believed to occur at the *roX* gene locus because roX RNAs are the only components of the complex being produced within the nucleus.

Based on both genetic and genomic analyses, the complex is thought to first target genomic regions called high-affinity sites (HAS), which include the *roX* genes, and then to spread to lower-affinity sites. During this process, MOF acetylates histone H4 lysine 16 across the entire X chromosome, which ultimately upregulates transcription (Conrad and Akhtar, 2011). However, how HAS are organized to allow the complex to reach the whole X chromosome continues to be an enigma. The MSL complex preferentially binds to an active chromatin environment containing a consensus sequence motif, called the MSL recognition

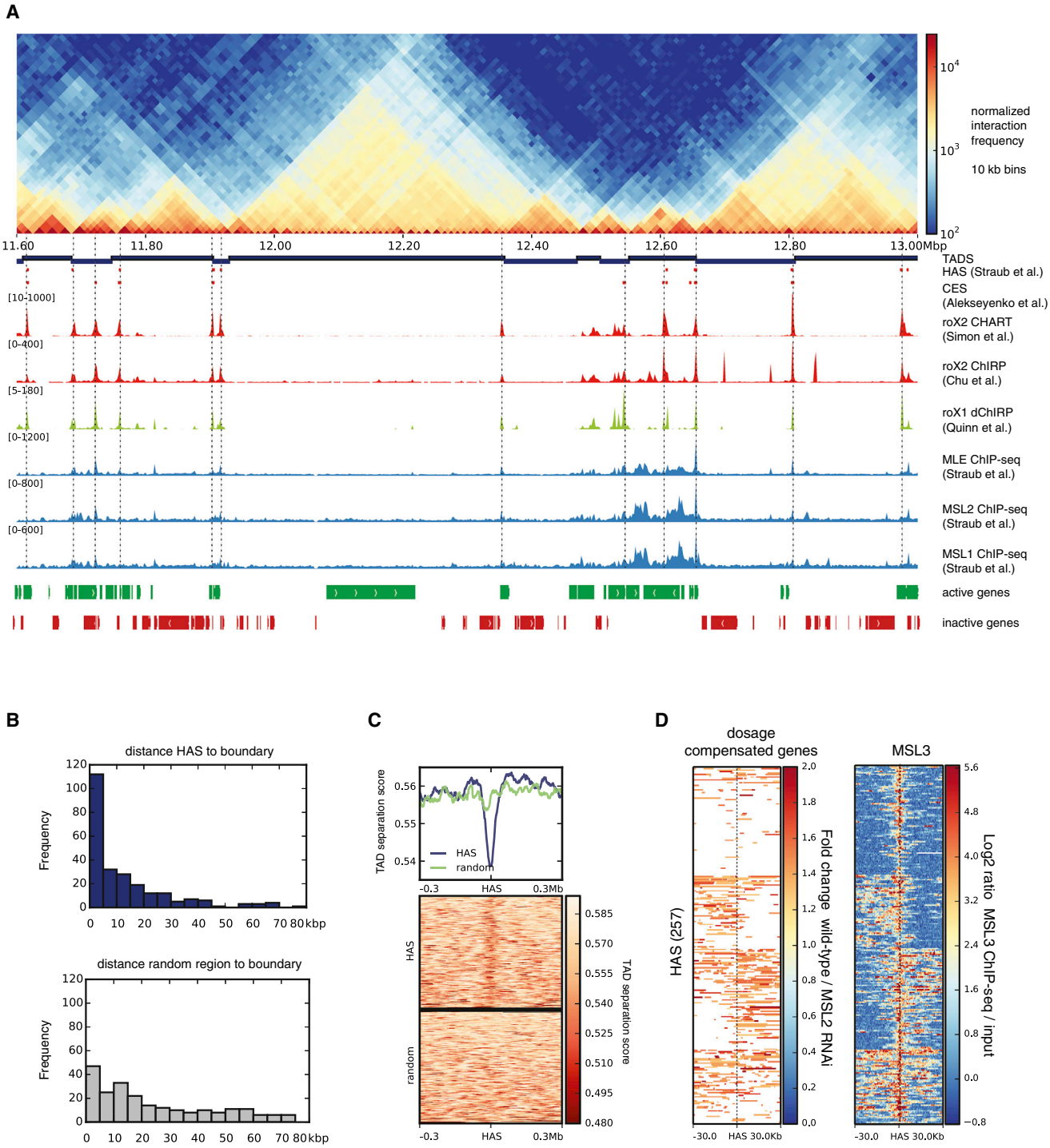

Figure 1. HAS Are Enriched at TAD Boundaries

(A) Normalized Hi-C counts at 10-kb resolution for the region 11.6–13.0 Mb in chromosome X of S2 cells. From the top, the tracks are as follows: partitioning of the genome into TADs; HAS as defined by Straub et al. (2008); HAS reported by Alekseyenko et al. (2008) (originally called chromosome entry sites [CESs]); roX2 CHART (Simon et al., 2011); roX2 ChIRP (Chu et al., 2011); roX1 domain-specific ChIRP (Quinn et al., 2014); MLE, MSL1, and MSL2 ChIP-seq (Straub et al., 2013); and active and inactive genes in S2 cells (Cherbas et al., 2011). Vertical lines are high-resolution HAS based on roX2 and MSL2 binding.

(B) Distribution of distances from the boundaries to HAS (top, blue) and from boundaries to the same number of shuffled random regions (bottom, gray) within chromosome X. The x axis represents the distance in kilobases from HAS to the boundary in bins of 5 kb. The y axis represents the number of HAS per bin.

(C) TAD separation score (Supplemental Experimental Procedures) around HAS showing the tendency of the MSL complex to land at boundaries. Lower scores indicate better TAD separation.

(legend continued on next page)

element (MRE), that is flanked by sequences of elevated GC content (Alekseyenko et al., 2012; Conrad and Akhtar, 2011). However, these features, although moderately enriched on the X chromosome, are also found on autosomes, and, therefore, it has not been possible to fully characterize HAS. Current models are based on linear genomic analysis or DNA fluorescent in situ hybridization (DNA FISH) on a few individual loci (Grimaud and Becker, 2009) without accounting for the potential influence of global chromosome conformation.

In this study, we used genome-wide chromosome conformation capture (Hi-C), a technique that enables the study of all chromosomal interactions within a genome at once (Lieberman-Aiden et al., 2009). This was further complemented by circularized chromosome conformation capture followed by deep sequencing (4C-seq) (Splinter et al., 2012) and three-dimensional double label DNA FISH (3D DNA FISH) analysis on single cells to study the interaction patterns of individual loci on the X chromosome. Our data highlight a distinct mechanism in flies in which specific features at topologically associating domain (TAD) boundaries on the X chromosome provide an advantageous location for the MSL complex to spread to spatially close regions and induce dosage compensation. Moreover, we show that, rather than modifying global chromosomal domain organization, the MSL complex acts locally by inducing chromatin remodeling at HAS.

RESULTS

High-Affinity Sites Occur Preferentially at Boundaries of Topologically Associating Domains

Previously published Hi-C studies in fruit flies could not address male-specific dosage compensation because either sex-mixed embryos (Sexton et al., 2012) or the female Kc cell line (Hou et al., 2012) alone were used. Therefore, we generated wild-type Hi-C contact maps using the restriction enzyme HindIII for two widely used male model cell lines, CME W1 cl.8+ (Currie et al., 1988) (clone-8) and Schneider's line 2 (Schneider, 1972) (S2) in biological duplicates. To ensure consistent comparisons, we also reprocessed previously published Hi-C contact maps for mixed-sex embryos and for Kc cell lines using the same mapping and normalization procedures (Figures S1A and S1B; Table S1). The correlation within replicates was very high for raw and corrected Hi-C counts (0.96 Pearson correlation in both cases, Figures S1C–S1F) as was the correlation between different cell types when raw and corrected Hi-C counts were considered. For the corrected counts we see an expected power-law decay of interaction frequencies with increasing genomic distance (Hou et al., 2012; Lieberman-Aiden et al., 2009; Sexton et al., 2012) and a similar decay for all chromosomes in the different Hi-C datasets (Figures S1G–S1I).

When combining our Hi-C data for S2 cells with published high-resolution roX occupancy sites (indicative of HAS) from capture hybridization analysis of RNA targets (CHART) (Simon et al., 2011) and chromatin isolation by RNA purification (ChIRP) (Chu et al., 2011) for this cell type, we observed that HAS have a tendency to localize at or near TAD (Dixon et al., 2012; Hou et al., 2012; Nora et al., 2012; Sexton et al., 2012) boundaries on the X chromosome. This can be seen readily by simple visual inspection of the data (Figure 1A; Figures S2A and S2B). To corroborate this finding, we used a domain caller (Experimental Procedures; Figures S3A–S3C) to define TAD boundaries in S2 and clone-8 cells. Because the TAD structure is highly conserved between the cell types studied (Figure S3D), the boundaries obtained for S2 and clone-8 cells are very similar to the published domain partitions for Kc (Hou et al., 2012) and *Drosophila* embryos (Sexton et al., 2012; Figures S3E and S3F). For the X chromosome, we identified a total of 257 HAS using the genome-wide mapping of roX2 (Simon et al., 2011) and MSL2 (Straub et al., 2013) (see also Table S2 and Supplemental Experimental Procedures). This association to TAD boundaries is significantly different from a random distribution ($p = 1.9 \times 10^{-11}$, Fisher's exact test, on the number of overlaps between boundaries and HAS; Supplemental Experimental Procedures). We found that 68% of HAS lie within a 20-kb distance of the nearest boundary. When calculated within a 5-kb distance, 45% of HAS are located near a boundary, in contrast to 9% expected by chance (Figure 1B; Figure S3G). To further validate this finding, we computed the TAD separation score at each HAS (Supplemental Experimental Procedures; Figures S3A and S3B) and verified that it tends to have a minimum, which is indicative of boundary regions, at HAS (Figure 1C). For comparison, similarly low values are obtained when the TAD separation score is evaluated at architectural protein binding sites (APBSs) (Van Bortle et al., 2014), which are thought to localize at TAD boundaries (Dixon et al., 2012; Hou et al., 2012; Sexton et al., 2012; Sofueva et al., 2013; Van Bortle et al., 2014; Figure S3H). When studying dosage-compensated genes (measured by downregulation of expression upon MSL2 depletion; Zhang et al., 2010), we found that they appear frequently either upstream or downstream of HAS (Figure 1D) in a pattern similar to the one observed for TAD boundaries that separate active and inactive chromatin (Figure S3I). Taken together, we conclude that the apparent linear arrangement of HAS along the genome follows a particular pattern dictated by the 3D TAD organization.

HAS Show More Enriched Hi-C Contacts in a Sex-Independent Manner

Previous analyses of Hi-C data have shown that active chromatin regions tend to interact (Lieberman-Aiden et al., 2009; Sexton et al., 2012). Moreover, boundary regions have been shown to be enriched in Hi-C contacts (Hou et al., 2012; Rao et al., 2014), and long-range contacts between architectural proteins have also been suggested (Liang et al., 2014). Because HAS are frequently associated with active chromatin (Alekseyenko et al., 2012) and appear at boundaries, we explored the possibility that the spreading in *cis* of the MSL complex could be mediated by long-range associations of HAS. Using a method similar to the paired end spatial chromatin analysis (PE-SCAn) (de Wit et al.,

(D) Dosage-compensated genes (based on RNA-seq data from wild-type and MSL2 RNAi-treated S2 cells; Zhang et al., 2010) and MSL3 ChIP-seq (Straub et al., 2013) up to 30 kb away from HAS. For dosage compensation, only genes showing activity are colored. The heatmap rows were divided into four clusters based on the kmeans algorithm using deepTools (Ramírez et al., 2014).
See also Tables S1 and S2 and Figures S1, S2, and S3.

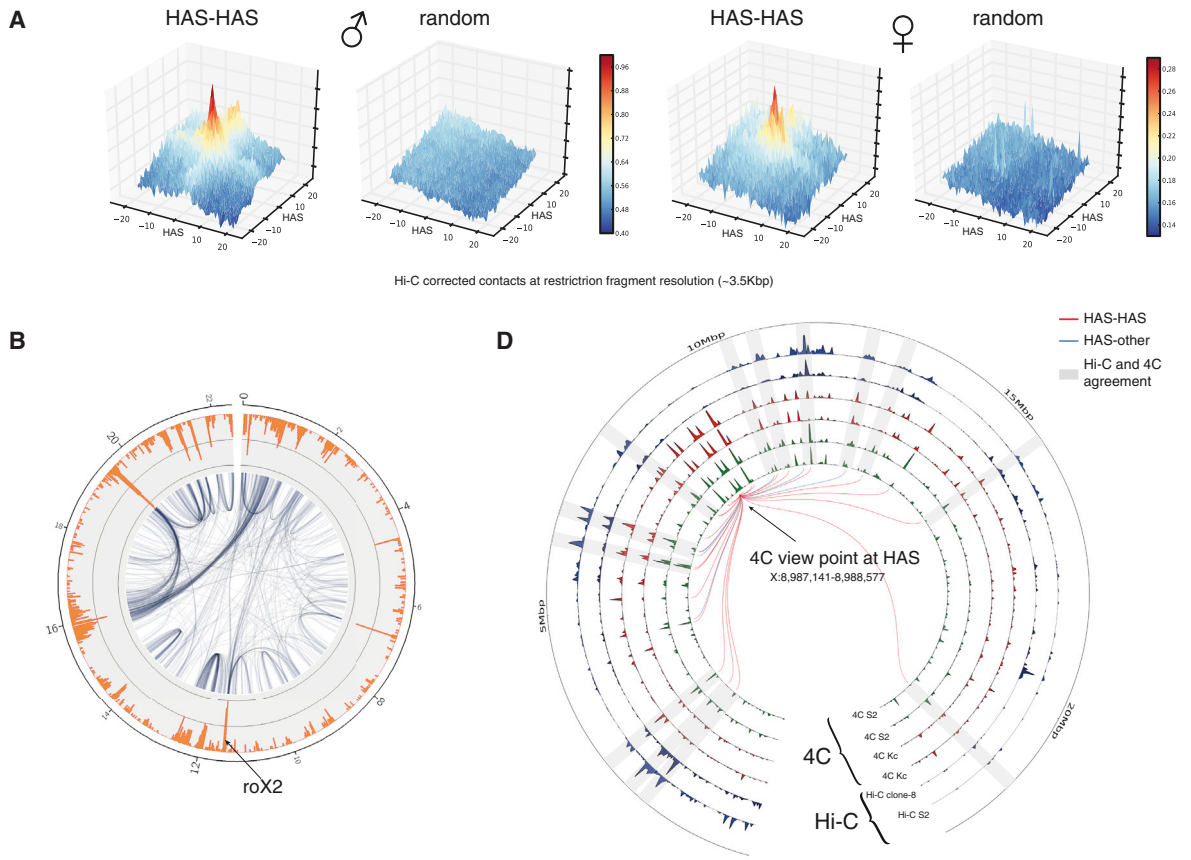

(legend on next page)

2013; Figure 2A), we found that HAS, and, in general, TAD boundaries on all chromosomes, are frequently enriched for Hi-C contacts in different cell lines, including female Kc cells (Figure 2A; Figures S4A and S4B). We also investigated the differences of *cis* long-range contacts on the X chromosome for each cell type and compared them with each other using a rigorous estimation of significant long-range Hi-C contacts (Figure 2B; Figures S4C and S4D; Supplemental Experimental Procedures). To gain statistical confidence and to avoid spurious results, we segmented the genome into 25-kb bins for this analysis. Our results revealed that HAS tend to exhibit more long-range contacts than other regions. HAS were found in 26% of the 25-kb bins on the X chromosome, and these regions contribute to 57% of all significant intra-X chromosomal long-range Hi-C contacts (Figure 2C). The spatial association between different HAS is highly significant because only 77 interactions (11%) are expected by chance ($p = 5 \times 10^{-16}$, Fisher's exact test, one-tailed). Similar results were found for all studied cell types when using different p value thresholds to call long-range contacts and for boundaries on other chromosomes (Table S3). The same analysis using 10-kb bins from a merge of all Hi-C samples for S2 cells (Supplemental Experimental Procedures) show comparable results (Figure S4E; see also Figure S4F for examples of enriched HAS-HAS contacts). Because the Hi-C results represent population averages where each cell may contain a unique chromosomal conformation (Nagano et al., 2013), we do not expect that all enriched HAS contacts are found in each cell but, rather, that HAS form a dynamic interaction network on the X chromosome. We analyzed long-range contacts for bins containing either a HAS and a boundary, a HAS only, or a boundary only. We found that bins that contained a HAS (either alone or together with a boundary) had, on average, more long-range contacts than the bins that only contained a boundary (Figure S5A). We additionally compared bins containing a boundary on the X chromosome with those on autosomes and found the average number of enriched contacts to be similar. Although the majority of HAS were in the same bins as boundaries, all bins that contained a HAS had, on average, more long-range contacts as the bins that only contained a boundary but no HAS (Figure S5A). This result suggests that HAS tend to be associated to boundaries with more long-range contacts.

We validated our Hi-C results using 4C-seq on male S2 and female Kc cell lines (for 4C viewpoints, see Table S4). Figure 2D and Figure S5B show comparisons of adjusted p values where the high correspondence between Hi-C and 4C can be seen. These comparisons show that our estimations of long-range contacts are reliable and can be reproduced by a different experimental and processing method as the one used for Hi-C. Furthermore, the 4C data allowed us to explore the enriched contacts at short genomic distances (5–10 kb) that are not possible with Hi-C. At this resolution, we consistently detect HAS-HAS-enriched contacts that remained unchanged between the male and female cell lines (Figure 2E; Figure S5C).

Depletion of MSL2 or MSL3 Does Not Change Global TAD Organization

The similarity between male and female results from Hi-C and 4C experiments suggested that, contrary to expectations (Grimaud and Becker, 2009), the MSL complex may not alter the conformation of the X chromosome. To directly investigate this, we generated Hi-C data in male S2 cells depleted of the MSL complex members (via RNAi-mediated knockdown of either MSL2 or MSL3; Figure S6A) and compared it with control knockdown (EGFP RNAi) or wild-type Hi-C samples. The resulting Hi-C counts showed a high correlation between all samples (Figure S6B), whereas the HAS-HAS-enriched contacts of the knockdown samples did not differ from those of the wild-type or EGFP RNAi control (Figure S6C; Table S3), and the TAD structure remained virtually identical (Figure S6D). These data indicate that the dosage compensation machinery in *Drosophila* does not broadly alter chromosomal topology but, rather, acts over a pre-existing chromosome conformation independent of sex.

Figure 2. HAS Show More Hi-C and 4C Ligations with Other HAS

(A) Enrichment of Hi-C contacts between HAS loci in male (S2) and female (Kc) data (Experimental Procedures). The x and y axes show the distance from HAS in restriction fragment resolution. The z axis contains the mean value of all pooled normalized sub-matrices corresponding to a HAS-HAS intersection.

(B) Representation of long-range Hi-C contacts from S2 cells as a network (25-kb bins, $p < 0.05$; Experimental Procedures). The orange outer rim shows the total number of long-range Hi-C contacts per bin.

(C) Quantification of long-range interactions on chromosome X from HAS to HAS (red), from HAS to other regions (green), and within other regions (dark blue). Multiple HAS found in the same bins were considered once.

(D) Comparison of enriched 4C contacts in males and females and Hi-C contacts in two cell lines for the viewpoint at HAS position X:8,987,141–8,988,577. Tracks displayed from outside toward the inside are as follows: Hi-C S2- and Hi-C clone-8-adjusted –log(p values) for a 25-kb binning; 4C contact enrichment –log(p values) for Kc replicate 1, Kc replicate 2, S2 replicate 1, and S2 replicate 2 at 25-kb binning. Lines represent enriched contacts detected in one of the 4C S2 replicates. Red lines indicate interactions between HAS, and the blue line indicates interactions from HAS to other regions. Peripheral numbering indicates the genomic position in megabases. Grey rectangles highlight the agreement between Hi-C and 4C at the enriched 4C contacts at the connecting lines. Close to the viewpoint, the detection of enrichments that are close to TAD size is limited when using Hi-C data.

(E) 4C data for a viewpoint at the end of gene *CG7766* confirms the interaction between two HAS that are 50 kb apart. Further 4C examples are shown in Figure S5C.

(F) Graph representing the location of HAS on different regions in and around genes.

(G) Enrichment of MREs bound by the MSL complex in contrast to the genome-wide background occurrence of MREs.

(H) TRAP score for MREs on autosomes (non-bound A), MREs not bound by the MSL complex on chromosome X (non-bound X), and MREs bound to the MSL complex (bound).

(I) Occurrence of MREs at different chromosomes filtered by the following criteria. The MRE has to be on active chromatin, determined using H3K36me3 (GEO: GSM685608), the MRE has to be located near the gene end, the MRE needs to have a TRAP score of at least −2, and the MRE should be located within 25 kb of the nearest boundary. MREs on chromosome X are enriched for these features.

See also Tables S3 and S4 and Figures S4 and S5.

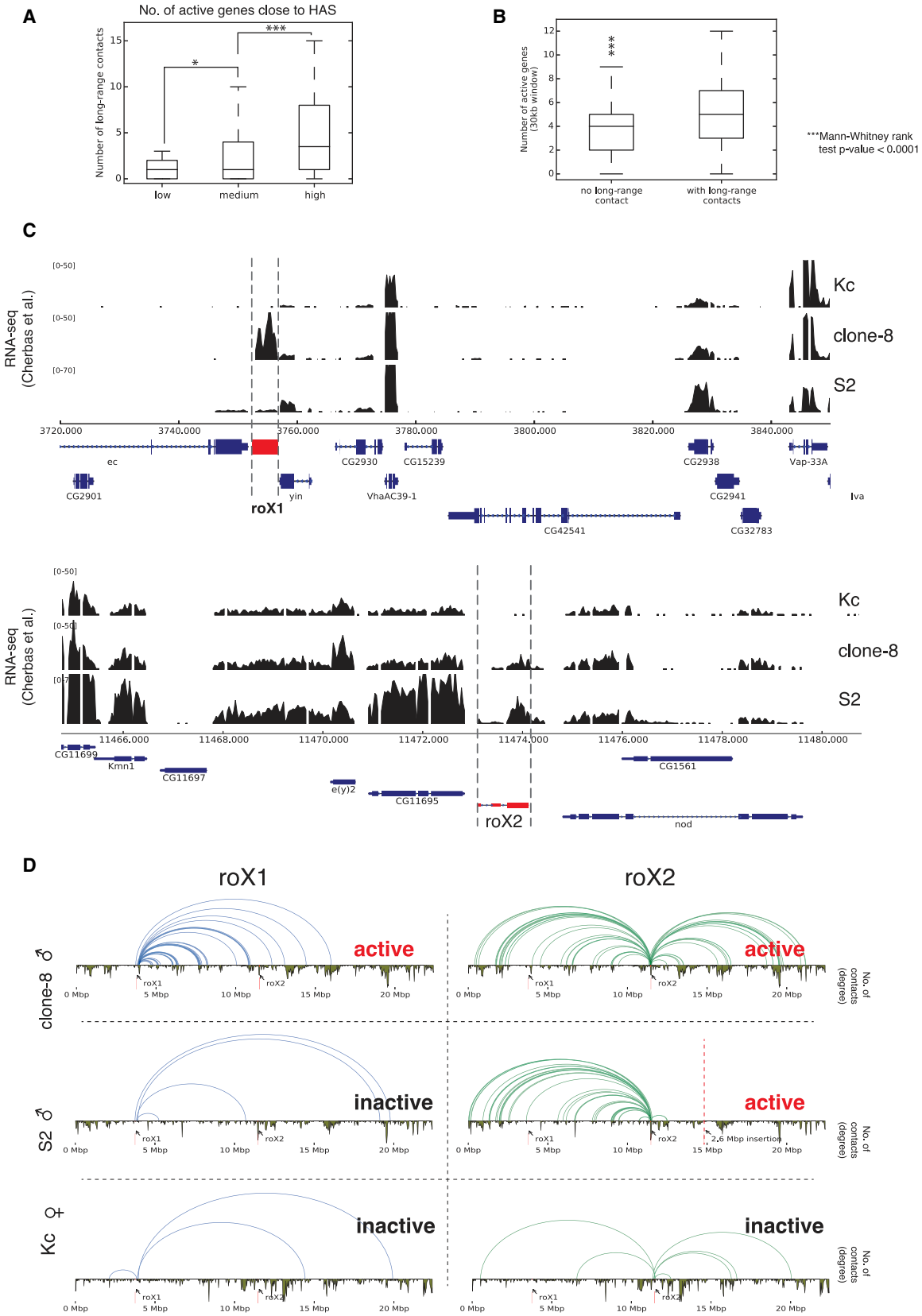

(legend on next page)

The X Chromosome Harbors Stronger MREs at Boundaries Compared with Autosomes

Because TAD boundaries are present on all chromosomes and are frequently enriched for long-range contacts (Figure S4B), we next addressed the relationship between TADs and HAS located on the X chromosome. Previous lower-resolution approaches have shown that HAS tend to be located at gene bodies or at the end of genes (Alekseyenko et al., 2008; Gilfillan et al., 2006). Using the high-resolution HAS derived from the CHART (Simon et al., 2011) and ChIRP (Chu et al., 2011) methods, we observe that HAS often appear on intronic regions (35%) and in the proximity of gene ends (51%), which include the 3′ UTR exon and convergent gene ends (Figure 2F). Moreover, HAS are almost never found at coding exons. The genomic distribution of the MRE associated to HAS over the different gene annotations revealed that gene ends are significantly enriched for MREs that are bound by the MSL complex (i.e., HAS) (Figure 2G). Also, HAS are always associated with active genes decorated with the histone H3 lysine 36 trimethylation (H3K36me3) histone mark and tend to have a DNA sequence with higher binding energy (transcription factor affinity prediction [TRAP] score; Thomas-Chollier et al., 2011), containing usually several copies of the MRE. When we considered only MREs that are at gene ends, are in active chromatin, have a log (TRAP score) of higher than −2, and are within 20 kb of the nearest boundary, we found that such a combination of features is enriched on chromosome X (Figures 2H and 2I). These data suggest that a combination of MREs, chromatin state, and gene architecture is required for the specificity of the MSL complex toward the X chromosome.

Differential Positioning of Active Regions within the X Chromosomal Territory

Correlation of expression and long-range contacts revealed that transcriptionally active HAS show more contacts compared with HAS located within inactive genes (Figures 3A and 3B). Analysis of two prominent HAS, *roX1* and *roX2*, allowed us to explore this finding in more detail. In clone-8 cells, both roX RNAs are actively transcribed (Cherbas et al., 2011), whereas more than 99.5% of S2 cells do not show roX1 expression (Johansson et al., 2011), and female Kc cells do not express any of the *roX* genes (Cherbas et al., 2011). In contrast, genes surrounding *roX1* and *roX2* are expressed similarly in the three cell lines (Figure 3C). We observed a greater number of long-range contacts when the *roX* genes are active (Figure 3D; Figures S6E and S6F), although no changes were seen on the TAD structure. Next we explored whether this difference between the two *roX* loci in the number of long-range contacts is reflected by their nuclear positioning in individual cells. For this, we performed 3D DNA FISH for *roX1* and *roX2* in clone-8 and S2R$^+$ cells (a derivative of the original S2 cells with a similar transcriptional profile) and measured the radial distances of the probes to the center of mass of the MSL1-immunostained region (MSL territory) (Figure 4A; Table S5). In clone-8 cells, both expressed *roX* genes showed almost equal distance distributions, whereas, in S2R$^+$ cells, the non-expressed *roX1* appeared to be farther away compared with the expressed *roX2* ($p = 1.9 \times 10^{-4}$, t test, one-tailed) (Figure 4B). In clone-8 cells, both roX probes can be found almost equally often outside of the MSL territory (17% of *roX1* and 14% of *roX2* signals), whereas, in S2R$^+$ cells, *roX1* is found outside more than three times as often as *roX2* (28% versus 8%, Figure 4C). Taken together, the differences in the relative locations of *roX1* and *roX2* with respect to the MSL territory in clone-8 and S2R$^+$ cells suggest that such positioning is related to their transcriptional activity. Consistent with this hypothesis, we observed that a FISH probe over a non-HAS (*dpr8,* inactive gene) was more frequently found outside of the MSL territory in comparison with two different HAS (HAS1 and HAS2, active genes) with respect to *roX2* (Figure 4D). These data suggest that differential positioning of active regions within chromosomes could serve as an elegant mechanism for tissue-specific fine-tuning without changes in TAD structure, therefore providing plasticity for gene regulation while maintaining stability of the overall chromosome shape.

The MSL Complex Spreads from HAS to Spatially Proximal Regions

Knowing that HAS are located at regions often engaging in long-range contacts, we tested whether this is a sufficient condition for targeting of the MSL complex to loci in 3D proximity to the *roX* genes by studying a previously unnoticed, large (~2.67-Mb) insertion of chromosome 3L (chr3L, ~796,745–3,468,912) into the X chromosome (chrX, ~14,809,484) that was revealed by our Hi-C analysis of S2 cells (Figure S7A) and is most likely present in one of the two X chromosomes in the tetraploid S2 cells. This large region appears to be enriched for the MSL3 protein—a hallmark of MSL complex spreading in chromatin immunoprecipitation sequencing (ChIP-seq) data.—although we did not detect typical HAS. In Figure 5A, we only see seemingly spurious roX peaks that are not consistent between the two methods used to determine roX-DNA contacts (CHART, Simon et al., 2011; ChIRP, Chu et al., 2011) and did not observe other MSL proteins. For comparison, an X-linked region of similar size as the insertion contains, on average, 30 HAS. Using a

Figure 3. Comparison of Gene Expression Activity and Long-Range Contacts

(A) Comparison of the number of active genes associated to HAS and the number of long-range contacts. We stratified the number of active genes within a 15-kb window up- and downstream of HAS into low (<4 active genes), medium (between 4 and 7 active genes) and high (8 or more active genes). *$p < 0.01$, ***$p < 0.0001$, Mann-Whitney rank test.

(B) Number of active genes in the vicinity (±15 kb) of HAS with or without long-range contacts.

(C) Gene expression (Cherbas et al., 2011) RNA-seq for genes close to *roX1* and *roX2*. In clone-8 cells, *roX1* and *roX2* are active, whereas, in S2 cells, only *roX2* is active.

(D) Schematic of long-range Hi-C contacts originating either from the *roX1* (±25 kb) or the roX2 locus (±25 kb) in clone-8, S2, and Kc cells. The activity status for each of the *roX* genes is shown in the respective panels. Complementary images showing 4C contacts can be found in Figures S6E and S6F.

See also Figure S6 and Table S4.

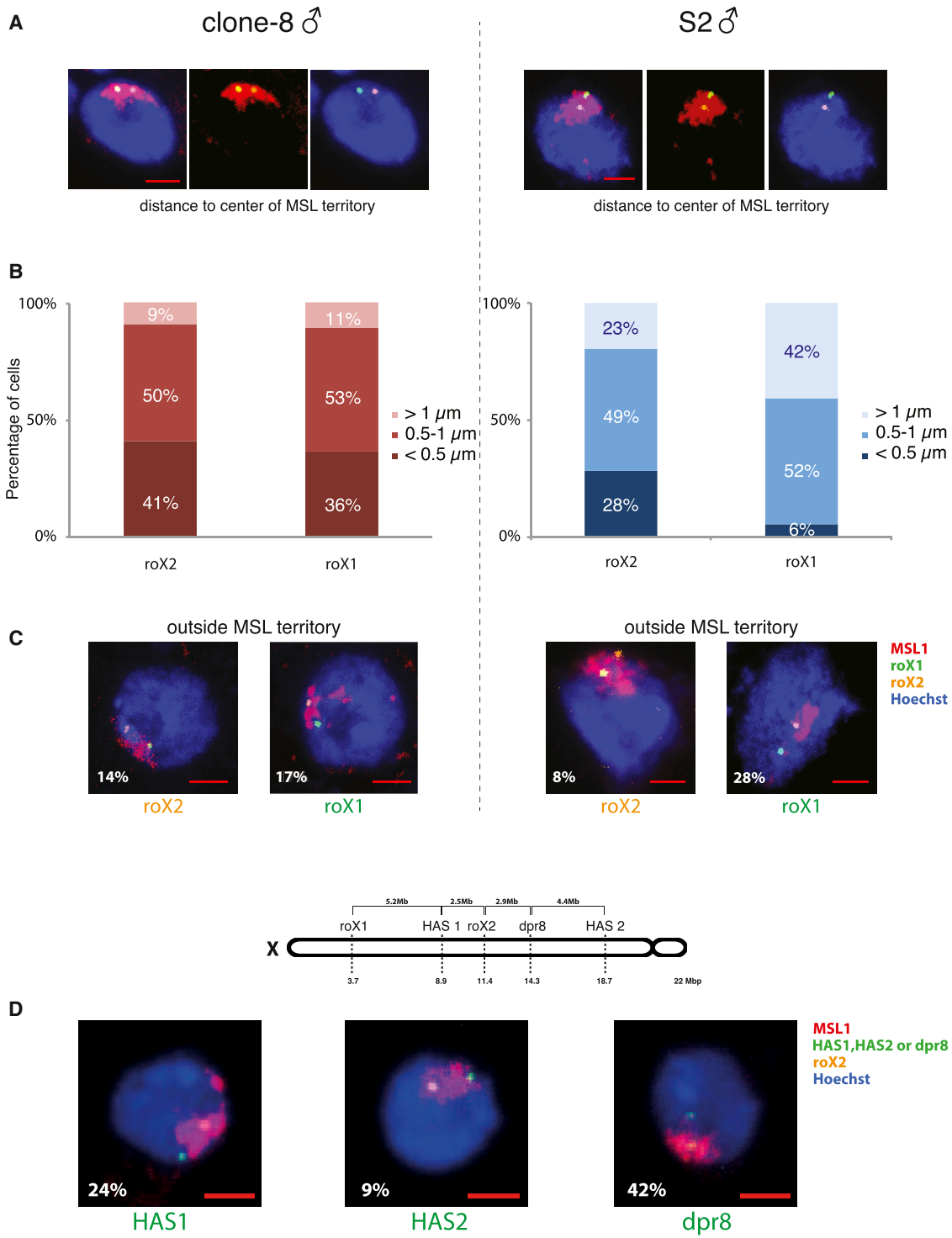

Figure 4. Differential Positioning of HAS Relative to the MSL Territory

(A) Representative maximum intensity projections of confocal image stacks of 3D FISH experiments with *roX1* (green) and *roX2* (orange) probes in S2R$^+$ and clone8 male *D. melanogaster* cells. MSL1 immunostaining is shown in red, and DNA is counterstained with Hoechst (blue). Scale bar, 2 μm.

(B) 3D distances from the center of mass of probes to the center of mass of the MSL territory. Graphs show the distribution of *roX1* and *roX2* probes in the different bins within the two cell lines: clone-8 (left) and S2R$^+$ cells (right).

(C) Percentage of cells in which either *roX1* or *roX2* are localized outside the MSL territory, as demarcated by MSL1 immunostaining, in clone-8 (left) and S2R$^+$ cells (right). Scale bars, 2 μm. n = 64 for clone-8 cells and 71 for S2R$^+$ cells.

(legend continued on next page)

4C viewpoint on the translocated region, we observed long-range contacts with the X chromosome. The same viewpoint in Kc cells, lacking this translocation, did not show any contacts (Figure S7B). These data demonstrate that, by being physically associated to the X chromosome, the MSL complex can spread via long-range contact over a region lacking HAS.

The MSL Complex Can Target a HAS Independent of the Proximity of the roX RNA Production Site

As a testable prediction following the above observations, we expected that autosomes would also display MSL spreading when a *roX* gene is placed in the appropriate region. In an adaptation of a classical rescue experiment (Meller and Rattner, 2002), we next generated transgenic flies carrying as a sole source of roX lncRNA a *roX2* insertion on the right arm of the third chromosome (3R) at a precise position (86F8) in a *roX1/2* double mutant background. The inserted *roX2* gene was complemented with an array of lac operon sequences and an EGFP-fused lacI as a reporter to visualize the transgene without the need of DNA FISH (Supplemental Experimental Procedures). Consistent with previous reports (Kelley et al., 1999), roX RNA produced from the autosomal *roX* insertion properly targeted the X chromosome, enabling functional dosage compensation and restoring male viability. Moreover, the *roX* transgene was able to recruit the MSL complex to the ectopic insertion site, where, in addition to local spreading of the MSL complex into direct flanking regions on the autosome (seen in salivary gland polytene chromosomes), we repeatedly detected MSL binding at band 88B on the third chromosome (Figure 5B). Interestingly, this cytological position resides ~2.6 Mb away from the insertion site, with no detectable binding within an ~1.7-Mb region in between targeted bands, supporting an involvement of the 3D conformation. Although S2 and clone-8 cells are not expected to share the 3D structure of polytene chromosomes, it is quite remarkable that, out of many other possibilities, we detect an enrichment of Hi-C contacts in S2 (Figure S7C) and clone-8 cells (data not shown) between 86F and 88B. This suggests that HAS (such as *roX* loci) enable spreading of the MSL complex to interaction sites that can be far away on a linear scale and that do not necessarily need to be HAS themselves. We further confirmed this observation by two independent approaches involving the ectopic expression of *roX1* and *roX2* genes from an autosomal location (VK33 on chromosome 3L) in the roX1/2 double-null background: insertion of UAS-driven *roX1* or *roX2* genes and translocation of an X chromosomal segment containing either *roX1* or *roX2* genes to the ectopic site. In all cases, the autosomally expressed roX fully rescued male lethality and induced MSL targeting to the X chromosome, as seen in polytene chromosome spreads (Figure 5C). A non-functional roX RNA lacking important stem loop structures and expressed from VK33 under its native promoter, on the other hand, was not able to rescue male lethality and led to diminished or mis-targeting to the chromocenter (Ilik et al., 2013; Figure 5D; Figure S7D). These experiments verify that the properties of the ectopic *roX1/2* are independent of the promoter or location of the *roX* genes but require an intact roX structure.

It has been proposed that the X chromosomal territory forms in a self-organizing process around the *roX* genes by attracting HAS (Grimaud and Becker, 2010). However, such a model seems incompatible with the targeting of the X chromosome observed for polytene chromosomes in the previous experiments unless the autosomal *roX2* was looping into the X chromosomal territory to physically reach the X chromosome. To test this, we analyzed intact nuclei from the LacO-roX2 line where we observed the formation of a distinct additional MSL territory surrounding the ectopic insertion of *roX2*, frequently distant to the main MSL territory in three different tissues (salivary glands and fat body [examples of polytenic tissues] as well as imaginal discs [diploid tissue]) (Figure 5E). These results suggest that physical proximity is not necessary for the transfer of roX RNA from its production site to its targets on the X chromosome and that it can occur efficiently despite a possibly distinct 3D chromosome conformation of different tissues. Still, we also show that spreading to spatially proximal regions, situated at a long genetic distance, is possible because the extra MSL territory surrounding the insertion site appears discontinuous on polytene chromosome squashes (Figure 5B).

Ectopic Insertion of *roX*-HAS Leads to Transcriptional Upregulation of Neighboring Autosomal Genes In Vivo

To further investigate the spreading of the MSL complex from ectopic *roX2* HAS to nearby autosomal locations, we isolated RNA from flies with or without ectopic *roX2* HAS and measured the expression of ten genes upstream and ten genes downstream of the insertion site. Active genes surrounding the ectopic *roX2* HAS showed a consistent upregulation of expression in comparison with control flies (Figure 6A). To complement this analysis, we performed ChIP-seq with an antibody against MOF from the same transgenic larvae. On autosomes, MOF binds only to gene promoters, whereas, on the X chromosome, it also binds to gene bodies (Kind et al., 2008; Figure 6B, right). In transgenic flies carrying an ectopic *roX2*, MOF binds not only to the bodies of active genes surrounding the autosomal insertion point but also at a distance from it (Figure 6B, left and center). Importantly, we could detect MOF binding at the body of active genes up to 0.5 Mb upstream (Figure 6B) and 2 Mb downstream of the insertion site (data not shown). This suggests that the presence of a HAS on an ectopic autosomal location enables MOF to spread to proximal and distal regions on autosomes. To further validate the influence of ectopic *roX* insertion on the expression of neighboring genes, we also determined the expression of genes neighboring a different transgene used in this study (i.e., the X chromosomal translocation to 65B2 on chromosome arm 3L [VK33], where *roX2* is expressed under its native promoter)

(D) Three additional DNA FISH probes (*dpr8*, HAS1, and HAS2) were used in S2 cells, paired with roX2, to study their positioning with respect to the MSL territory. Representative pictures of each probe pair are shown, with the percentage of probes escaping the MSL territory indicated at the bottom left of each panel. Shown above is a schematic of the genomic location of all probes used in this study on the X chromosome of *D. melanogaster*. Scale bars, 2 μm. n = 45 for HAS1, for HAS2, and 30 for *dpr8*.
See also Table S5.

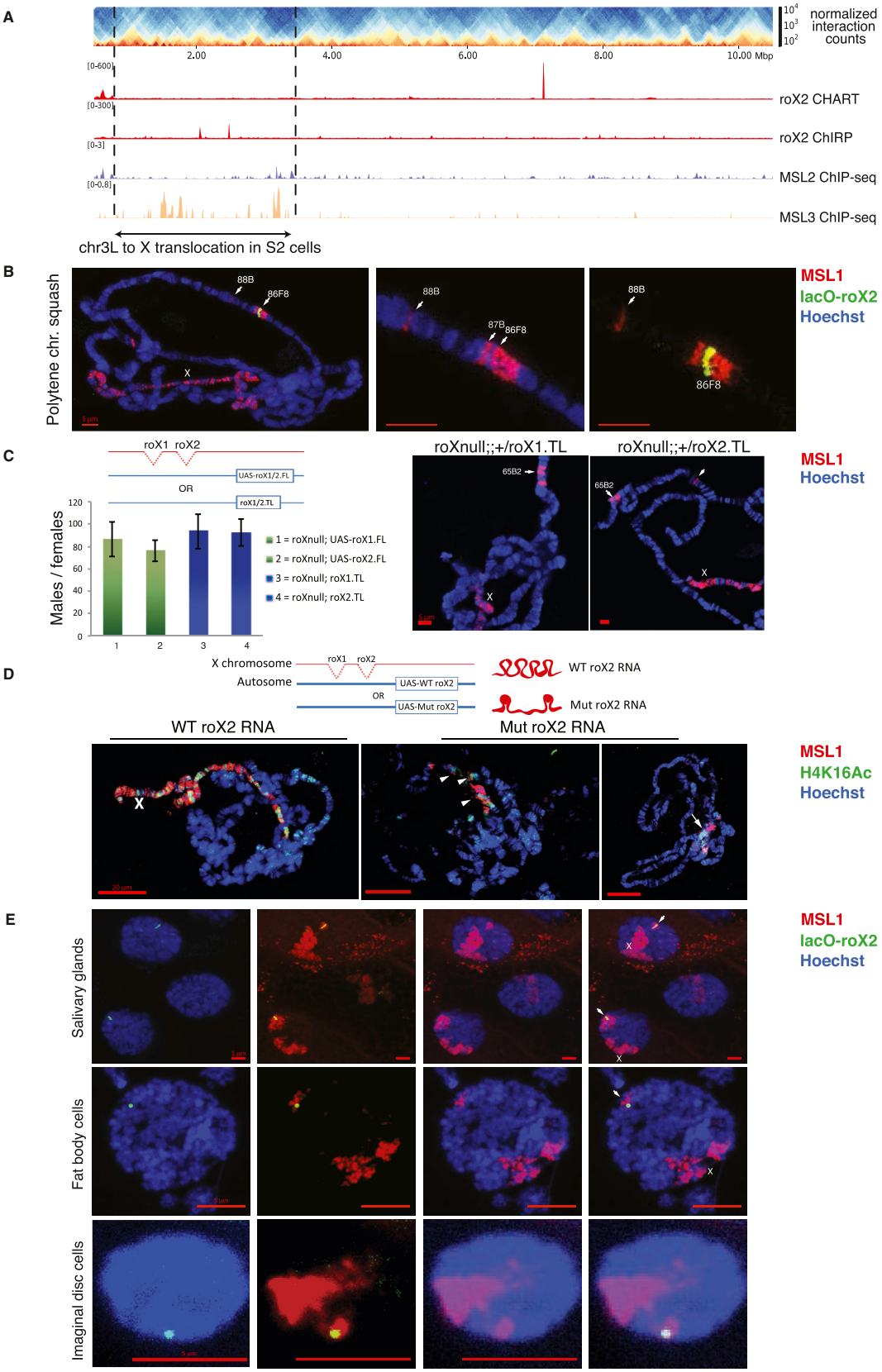

(legend on next page)

and also observed enhanced expression of ten genes surrounding this insertion site (Figure 6C). Taken together, these observations corroborate that the presence of a roX2 HAS enables the MSL complex to spread distally from the site of insertion and that it has activating potential on gene expression in vivo.

Nucleosome Positioning at HAS Is Dependent on the Presence of MSL2

Investigating functional HAS more closely, we observed that they tend to display increased DNaseI hypersensitivity (Figure S7E). We therefore asked whether the local chromatin structure of HAS can be influenced by the MSL complex. To this end, we mapped the positioning of nucleosomes in S2 cells by treating the chromatin with micrococcal nuclease, followed by deep sequencing (MNase-seq) (Mavrich et al., 2008). We found nucleosome-depleted regions on HAS, flanked by well positioned nucleosomes (Figure 7A). To test whether the MSL complex has any roles in maintaining the nucleosome configuration, we performed MNase-seq analysis in S2 cells depleted of MSL2. Strikingly, the nucleosome pattern around HAS was lost upon depletion of MSL2 ($p < 2.2e\text{-}16$; Supplemental Experimental Procedures), whereas it was preserved at the transcription start site (TSS). We conclude that the MSL complex is crucial for the maintenance of the local nucleosome arrangement, specifically at HAS.

DISCUSSION

This study provides a first step toward understanding the role of chromosome conformation in dosage compensation in *D. melanogaster*. We observe that HAS, the landing regions of the MSL complex on the X chromosome, frequently reside in proximity to TAD boundaries. We demonstrate that HAS are enriched in Hi-C contacts to each other and to other X chromosomal regions and that this organization remains comparable between male and female cells.

The Conformation-Based Affinity Model Explains MSL Complex Targeting and Spreading on the X Chromosome

Our analysis revealed that HAS are characterized by a combination of DNA sequence (MREs), chromatin state (active), and gene architecture, which drives the specificity of the MSL complex toward the X chromosome (Figure 7B, Targeting). Our data suggest that when the MSL complex binds to HAS, it then spreads (either via an active mechanism or via diffusion) to spatially close regions to place the histone H4 lysine 16 acetylation (H4K16ac) mark on active genes (Figure 7B, Spreading). We propose a "conformation-based affinity" model based on the strategic location of HAS at highly interconnected regions of the *D. melanogaster* X chromosome that efficiently distribute the MSL complex over the X chromosome by attracting the MSL complex to *cis*-interacting HAS on the X chromosome. This system ensures that only this chromosome is specifically and globally targeted. By spreading from those HAS over short (3D) distances, all active genes on the X chromosome are then reached and acetylated without influencing the autosomes. We suggest that this system is resilient to major perturbations, exemplified by the large autosomal insertion from chromosome 3L and the ectopic expression of the *roX* genes that produce viable cells and flies, respectively (Figure 5).

The MSL Complex Is Crucial for Maintaining Nucleosome-Free Regions at HAS

Our MNase-seq analysis shows, for the first time, a direct effect of the MSL complex on nucleosome organization specifically on HAS (Figure 7A) and not on the TSS, despite prominent binding of MSL1/2 to promoter regions. The MSL complex may act similar to a pioneer DNA binding protein (Magnani et al., 2011) to establish nucleosome patterns at HAS and may act on neighboring active regions rather than modifying TAD boundaries. This system may be unique to flies because the *Drosophila* dosage compensation evolved a fine-tuning transcription activation mechanism rather than a complete shutdown of gene transcription as seen in mammalian X chromosome inactivation. It would be very interesting to see how nucleosome positioning is affected upon Xist binding in mammals.

HAS Locate at Regions with Abundant Long-Range Contacts to Facilitate Spreading

Although many factors, including the CCCTC-binding factor (CTCF) as well as tRNA and housekeeping genes, have been shown to be enriched at boundaries (Dixon et al., 2012; Hou

Figure 5. Insertion of an Autosomal Fragment into the X Chromosome and of the *roX2* HAS into an Ectopic Autosomal Location

(A) Hi-C heatmap of chromosome 3L highlighting a 2.67-Mb translocation (chr3L, ~796,745–3,468,912) into chromosome X. Figure S7B shows 4C long-range contacts from the translocation to chromosome X.

(B) The autosomal insertion of LacO-roX2 (green) into 86F8 on chromosome arm 3R efficiently targets the MSL complex (MSL1, red) to the X chromosome in males and causes local spreading from the insertion site in polytene chromosomal immunostaining of salivary glands from male third-instar larvae. DNA is stained with Hoechst 33342 (blue). Figure S7C contains the Hi-C counts from the insertion point on band 86F8 in S2 cells. Scale bars, 5 μm.

(C) Left: rescue of $roX1^{SMC17A}$, $roX2^{\Delta}$ double mutant (roX^{null}) male-specific lethality by *daGal4*-induced expression from a full-length (FL) *UAS-roX1* transgene (#1) or *UAS-roX2* transgene (#2) or by expression driven by endogenous promoters upon translocation (TL) of *roX1* (#3) or *roX2* (#4) to the third chromosome. All transgenes are inserted in the same autosomal location (VK33). Transgenic males surviving to adulthood were counted and normalized to female siblings (100% viable, ~1,100 flies/genotype). Columns show averages of $n \geq 3$ separate crosses ± SD. See Experimental Procedures for details of the genetic crosses. Below the graph is a schematic of the transgenes used. Right: two representative polytene chromosome squashes are shown for roX^{null}; TLroX1/2. Scale bars, 5 μm.

(D) A mutant form of roX RNA lacking important stem-loop structures is expressed from the VK33 autosomal insertion. This causes inefficient targeting of the MSL complex (MSL1, red) to the X chromosome and mislocalization of H4K16 acetylation (green), as visualized on polytene chromosomal immunostaining of salivary glands from male third-instar larvae (see Supplemental Experimental Procedures and Figure S7D for further details). Scale bars, 20 μm.

(E) As (C) but showing intact nuclei of whole salivary glands (top), fat body cells (center), and imaginal disc diploid cells (bottom). X indicates the X chromosome, and arrowheads point to the region around the lacO-roX2 autosomal insertion. Scale bars, 5 μm.

See also Figure S7.

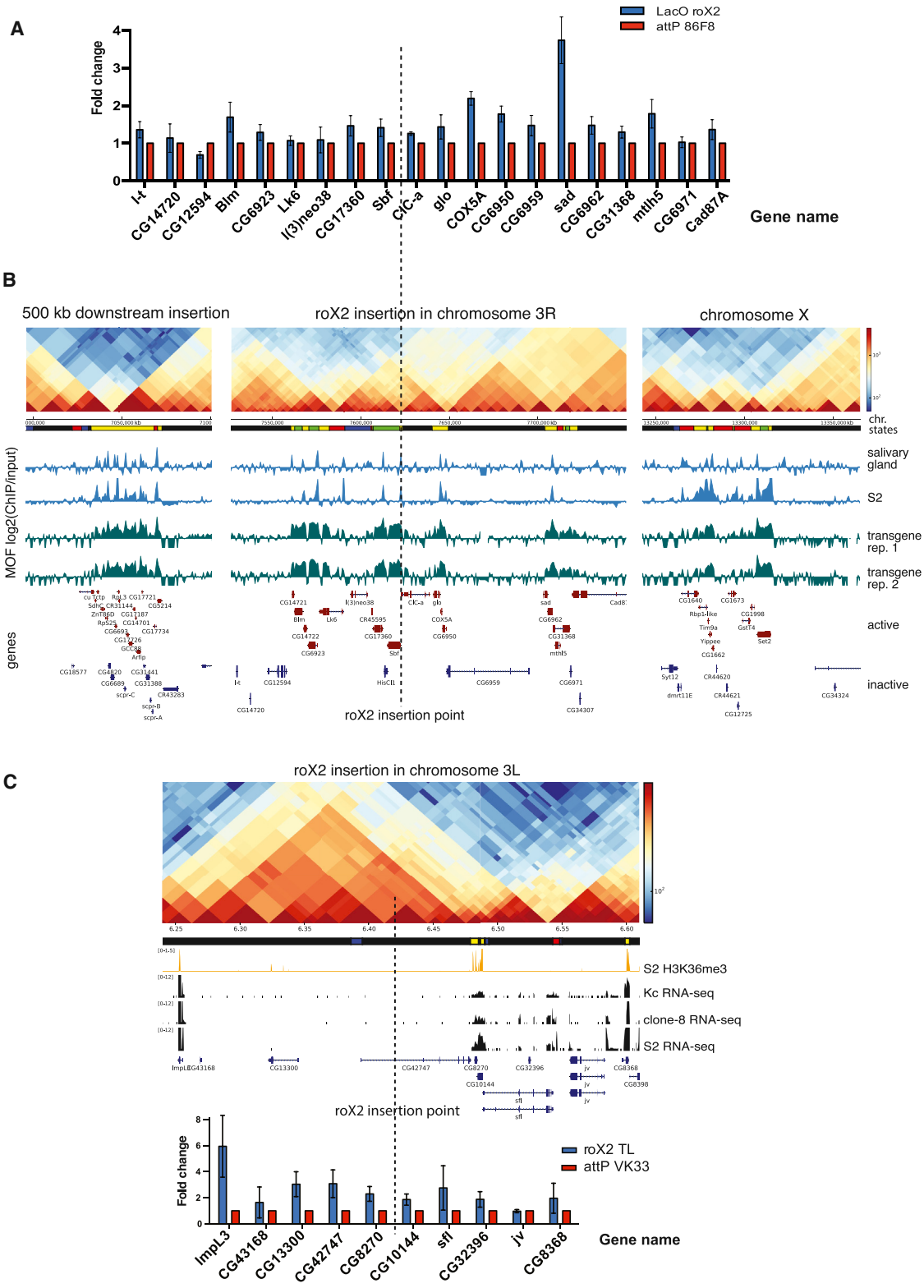

Figure 6. Ectopic Insertion of a HAS Leads to Spreading of MOF to and Enhanced Expression of Neighboring Autosomal Genes

(A) A HAS on a autosomal location causes an upregulation of autosomal genes. Expression of autosomal genes neighboring *roX2* insertion was analyzed by qRT-PCR. Flies analyzed were *roX* double mutant (*roX*^{null}) combined with either a transgene carrying LacO-roX2 (under the endogenous promoter, LacO-roX2, blue

(legend continued on next page)

et al., 2012; Sexton et al., 2012), by dissecting the targeting and spreading activity of the MSL complex for the X chromosome we offer a plausible explanation behind the advantages of HAS localization. HAS are enriched at the X chromosomal boundaries and not at autosomal boundaries, where all other boundary factors will bind indiscriminately. Furthermore, we found that the few HAS that are not near a boundary also occupy locations of an elevated number of long-range contacts (Figure S5A), indicating that HAS form interaction hubs for the spreading of the MSL complex.

Activity of *roX* Genes Is Associated with a Higher Abundance of Long-Range Contacts

Hi-C as well as in vivo immunofluorescence show that active *roX* genes have more contacts and are closer to each other than inactive regions (Figure 3). These observations are in line with previous reports showing that active chromatin compartments interact more often with each other (Lieberman-Aiden et al., 2009; Sexton et al., 2012) and that active chromatin localizes to the interface of the chromosomal territory (Nagano et al., 2013). Our results imply that different transcriptional programs in each cell line or tissue are likely to be associated with a particular arrangement of long-range contacts, suggesting that the dosage compensation must be flexible to act over such diverse conformations without disturbing them. This idea is consistent with the observation that the chromosome conformation remains unchanged after knockdown of the MSL complex (Figures S6A–S6D), and stays in contrast to mammalian X inactivation, which involves chromatin condensation, gene inactivation, and alterations in chromosome conformation (Nora et al., 2012).

lncRNAs Work Differently in Coordinating Fly and Mammalian Dosage Compensation

Dosage compensation mechanisms in flies and mammals lead to opposite outcomes; namely, gene activation versus gene repression. However, both systems use lncRNAs transcribed from the dosage-compensated X chromosome. roX1 and roX2 RNA are expressed from the male hyperactivated X chromosome in *D. melanogaster*, whereas Xist is expressed from the inactivated X chromosome in mammalian females (Brockdorff and Turner, 2015; Grimaud and Becker, 2010). Recent work has shown that Xist spreads to distal sites on the X chromosome. Interestingly, this spreading is dependent on the spatial proximity of sites distal to the *Xist* gene (Engreitz et al., 2013; Simon et al., 2013). This is further exemplified by ectopic expression of *Xist* from chromosome 21, where Xist spread only in *cis* on this chromosome (Jiang et al., 2013). In our study, ectopic insertion of *roX* transgenes on autosomes demonstrated that the roX/MSL complex can reach the X chromosome and rescue male lethality (Figures 5B–5D). Therefore, acting in *trans* is a special feature of roX RNAs (in conjunction with the MSL complex) not observed for Xist, indicating that the two systems utilize the respective lncRNAs differently. In both systems, however, the lncRNAs need to be functional because the stem loop structures of the roX RNAs are required for dosage compensation in *D. melanogaster* (Ilik et al., 2013; Figure S7D), whereas Xist needs the "A repeat domain" to induce mammalian X chromosome inactivation (Engreitz et al., 2013). The distinct mechanisms utilized by the Xist and roX RNAs exemplify the great versatility by which lncRNAs can be involved in the global regulation of single chromosomes and might reflect important differences between the two systems. In mammals, only one of the two X chromosomes needs to be inactivated. Therefore, a *trans* action of Xist RNA on the sister X chromosome would be detrimental to the organism. In contrast, the dosage-compensated X chromosome is present singularly in males in *Drosophila*. However, because the roX RNAs can act in *trans*, it may be disadvantageous to target the activating MSL complex to active genes on autosomes, hence the need for specific target regions (the HAS) unique to the X chromosome.

Faster Evolution of the X Chromosome May Favor Positioning of HAS to Interaction Hubs

To fully understand the occurrence of HAS at sites with extensive long-range interactions on the X chromosomes, it could be helpful to consider evolutionary models proposing that X chromosomes tend to evolve faster than autosomes (faster X effect) (Vicoso and Charlesworth, 2006). Under the faster X effect, traits only beneficial for males can introduce significant changes specific to the X chromosome on a short evolutionary timescale (Parsch and Ellegren, 2013; Vicoso and Charlesworth, 2006). Based on these and other observations suggesting that the X chromosome in flies is different from autosomes (Alekseyenko et al., 2012; Gallach, 2014; Meisel and Connallon, 2013; Zhang and Oliver, 2010), we assume that selective pressures on males favored the occurrence of HAS at regions of increased interactions, like TAD boundaries. Future analyses of different *Drosophila* species will open exciting opportunities to study the evolutionary changes of HAS in the context of X chromosomal architecture. Moreover, conformation-based affinity could be a

bars) or the attP transposon only in the same insertion site (AttP 86Fb, red bars). Relative gene expression levels of LacO-roX2 flies were calculated over that of AttP 86Fb flies. Data are represented as the mean of triplicates ± SEM. PFK levels were used as control.

(B) MOF spreads to distal regions from the *roX* insertion site on chromosome 3R. The tracks shown from top to bottom are as follows: Hi-C contacts from S2; chromatin states (Filion et al., 2010); input-normalized MOF ChIP-seq signals for third-instar larva salivary gland (Conrad and Akhtar, 2011); and S2 cells (Straub et al., 2013) and LacO-roX2 flies (two replicates). The Hi-C heatmap contains corrected counts from single restriction fragments. In the chromatin states track, the yellow and red regions represent active chromatin, black corresponds to repressive chromatin, and blue and green represent heterochromatin. The tracks are shown for a 100-kb region located 500 kb downstream of the *roX2* insertion site (left), a 250-kb region around the insertion site (center), and a 100-kb region on the X chromosome (right). The dotted line depicts the autosomal insertion site of *roX2* (chromosome 3R, 86F8).

(C) Expression of autosomal genes neighboring the *roX2* insertion was analyzed by qRT-PCR. Flies analyzed were *roX* double mutant (roX^{null}) combined with either a translocation of *roX2* (roX 2 TL) to an insertion site on chromosome 3L (VK33) or the attP transposon alone in the same VK33 insertion site. Relative gene expression levels (± SEM) of roX2 TL flies were calculated over that of AttP VK33 flies. Data are represented as the mean of triplicates ± SEM. PFK levels were used as control. Genes in repressive chromatin or heterochromatin have low or no upregulation (e.g., *CG14720* and *CG15594* in A and *CG43168* and jv in C). H3K36me3 and RNA-seq tracks are used to indicate gene transcription activities in different cell lines.

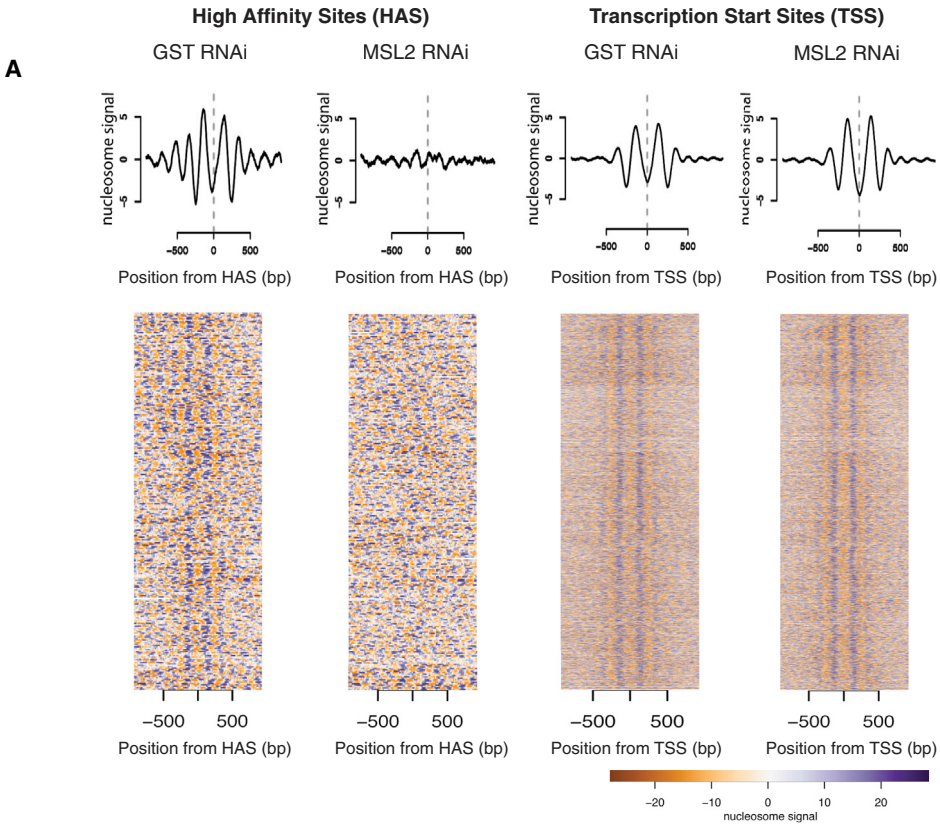

(legend on next page)

generic mechanism for other regulatory elements to exert their functions. It remains to be seen in which contexts the in *cis* versus in *trans* action of different lncRNAs is essential for their function and how chromosome conformation, long-range contacts, HAS, and regulation of transcription have co-evolved for dosage compensation.

EXPERIMENTAL PROCEDURES

Hi-C Experimental Procedure and Analysis

Hi-C in S2 or clone-8 cells using HindIII as restriction enzyme was carried out as described by Belton et al. (2012) with the following minor modifications. Starting material for all samples was 50 million insect cells/sample. After lysis, samples were taken up in 125 μl and split into two aliquots of 50 μl (Hi-C samples), and the remaining 25 μl (3C control) were used to adjust for the smaller size of the *Drosophila* genome compared with mammalian cells. Accordingly, for each 3C control, only half of the volumes per tube were used compared with the original protocol. For details, see Supplemental Experimental Procedures.

4C-Seq Experimental Procedure and Analysis

4C-seq in S2 and Kc cells was carried out as described by Splinter et al. (2012) with minor modifications as follows. 50–100 million S2 cells or Kc cells, fixed as described above, were used for two biological replicates. DpnII (New England Biolabs) was used as the primary and Csp6I (Thermo Scientific) as the secondary restriction enzyme. For each viewpoint, two 160-ng PCR reactions (8 cycles with a 55°C annealing temperature, followed by 18 cycles at 63°C) were prepared and cleaned up. All different viewpoint libraries for one biological replicate were mixed equimolarly and sequenced on separate lanes on an Illumina HiSeq2500 DNA sequencer. Primer sequences and coordinates for the experiments can be found in Table S4.

Fly Culture and Genetics

Details of fly culture conditions and genetics are explained in the Supplemental Experimental Procedures.

FISH

Fluorescence in situ hybridization procedures were performed as described previously (Vaquerizas et al., 2010). To perform DNA FISH, approximately ten 5-kb regions were chosen in the genome and amplified by PCR from genomic DNA with five to ten primers pairs, each covering around 0.5–3 kb. Primer sequences are available upon request. The roX1 probe sequence was taken from Vaquerizas et al. (2010). The *roX2* and *dpr8* probe sequences were taken from Grimaud and Becker (2009). The HAS1 and HAS2 probes were designed and generated for this study.

Nucleosome Positioning Analysis in *Drosophila*

Nucleosome positioning analysis using MNase-seq was performed essentially as described in Mavrich et al. (2008). For details of the analysis, see the Supplemental Experimental Procedures.

ACCESSION NUMBERS

The accession number for the Hi-C, 4C-seq, MNase-seq, and ChIP-seq raw and processed data reported in this paper is GEO: GSE58821.

Supplemental information

Supplemental information includes Supplemental Experimental Procedures, seven figures, and five tables and can be found with this article online at http://dx.doi.org/10.1016/j.molcel.2015.08.024.

AUTHOR CONTRIBUTIONS

Conceptualization, F.R., T.L., T.M., and A.A.; Methodology, F.R., T.L., S.T., and K.L.; Software, F.R.; Formal Analysis, F.R., T.L., S.T., K.L., and H.C.; Investigation, F.R., T.L., S.T., K.L., and P.G.; Resources, P.G., B.L., Y.Z., J.D., E.d.W., and W.d.L.; Data Curation, F.R. and B.L.; Writing – Original Draft, F.R., T.L., S.T., and A.A.; Writing – Review & Editing, F.R., T.L., S.T., K.L., E.d.W., W.d.L., T.M., and A.A.; Visualization, F.R., T.L., S.T., K.L., and A.A.; Supervision, W.d.L., J.D., T.M., and A.A.; Funding Acquisition, A.A.

ACKNOWLEDGMENTS

We thank all members of the A.A. laboratory for discussions and especially F. Dündar, A. Gaub, T. Aktas, T. Khanam, T. Chelmicki, I. Ilik, and N. Iovino for critical reading of the manuscript. We thank G. Arib and I. Ilik for generating the lacO-roX2 and UAS-roX1/2 fly lines, respectively; M. Shvedunova for initial help with imaging; A. Panhale for culturing clone-8 cells; and N. Gutierrez for support with the generation of FISH probes. We thank U. Bönisch and E. Betancourt for help with deep sequencing. This work was supported by EU-funded "EpiGeneSys" and DFG:CRC992 and DFG:CRC746 (to A.A.). A.A. is part of the DFG-funded BIOSSII excellence cluster.

Received: March 16, 2015
Revised: July 20, 2015
Accepted: August 25, 2015
Published: October 1, 2015

REFERENCES

Alekseyenko, A.A., Peng, S., Larschan, E., Gorchakov, A.A., Lee, O.-K., Kharchenko, P., McGrath, S.D., Wang, C.I., Mardis, E.R., Park, P.J., et al. (2008). A sequence motif within chromatin entry sites directs MSL establishment on the Drosophila X chromosome. Cell *134*, 599–609.

Alekseyenko, A.A., Ho, J.W.K., Peng, S., Gelbart, M., Tolstorukov, M.Y., Plachetka, A., Kharchenko, P.V., Jung, Y.L., Gorchakov, A.A., Larschan, E., et al. (2012). Sequence-specific targeting of dosage compensation in Drosophila favors an active chromatin context. PLoS Genet. *8*, e1002646.

Belton, J.-M., McCord, R.P., Gibcus, J.H., Naumova, N., Zhan, Y., and Dekker, J. (2012). Hi-C: a comprehensive technique to capture the conformation of genomes. Methods *58*, 268–276.

Figure 7. Depletion of the MSL Complex Severely Affects Nucleosome Positioning at HAS but not at the TSS

(A) Summary plots (top) and heatmaps (bottom) showing normalized nucleosome occupancy for regions centered around HAS (left, n = 257) and active TSSs (right, n = 5985) in control (GST RNAi) and MSL2-depleted cells (MSL2 RNAi). A bar representing the nucleosome signal is shown below.

(B) Conformation-based affinity model. We propose a model in which chromosome X is targeted via HAS by the MSL complex independently of spatial proximity (1). Then the complex spreads from the HAS to spatially proximal regions (2). In (1), the MSL complex binds specific regions of chromosome X containing a sequence motif (the MRE) if this appears at the end of active genes that are at TAD boundaries. In (2) the complex spreads (probably by diffusion) from HAS to spatially close regions. Because TAD boundaries appear enriched in contacts within each other as well as to other regions, it is expected that they are physically close, therefore offering an optimal location from which to reach all active genes on chromosome X.

(C) Comparison of the ectopic expression of roX RNA versus Xist RNA on autosomes. Blue arrows denote spreading of the lncRNA in 3D proximity, and orange arrows denote targeting of the lncRNA in *trans* (blue box). In *Drosophila*, ectopically expressed roX displays restricted spreading on the autosome, indicating that spatial proximity is beneficial, but not sufficient, for roX RNA spreading. Importantly, roX RNA expressed from an autosomal location specifically targets the X chromosome in *trans*, leading to coating of the entire X chromosome by the roX/MSL complex independent of spatial proximity (yellow box). In mammals, ectopically expressed Xist RNA can spread and coat the autosome using spatial proximity (Engreitz et al., 2013; Jiang et al., 2013; Simon et al., 2013) without targeting the X chromosome in *trans*.

See also Figure S7.

Brockdorff, N., and Turner, B.M. (2015). Dosage compensation in mammals. Cold Spring Harb. Perspect. Biol. *7*, a019406.

Cherbas, L., Willingham, A., Zhang, D., Yang, L., Zou, Y., Eads, B.D., Carlson, J.W., Landolin, J.M., Kapranov, P., Dumais, J., et al. (2011). The transcriptional diversity of 25 Drosophila cell lines. Genome Res. *21*, 301–314.

Chu, C., Qu, K., Zhong, F.L., Artandi, S.E., and Chang, H.Y. (2011). Genomic maps of long noncoding RNA occupancy reveal principles of RNA-chromatin interactions. Mol. Cell *44*, 667–678.

Conrad, T., and Akhtar, A. (2011). Dosage compensation in Drosophila melanogaster: epigenetic fine-tuning of chromosome-wide transcription. Nat. Rev. Genet. *13*, 123–134.

Currie, D.A., Milner, M.J., and Evans, C.W. (1988). The growth and differentiation in vitro of leg and wing imaginal disc cells from Drosophila melanogaster. Development *102*, 805–814.

de Wit, E., Bouwman, B.A.M., Zhu, Y., Klous, P., Splinter, E., Verstegen, M.J.A.M., Krijger, P.H.L., Festuccia, N., Nora, E.P., Welling, M., et al. (2013). The pluripotent genome in three dimensions is shaped around pluripotency factors. Nature *501*, 227–231.

Dixon, J.R., Selvaraj, S., Yue, F., Kim, A., Li, Y., Shen, Y., Hu, M., Liu, J.S., and Ren, B. (2012). Topological domains in mammalian genomes identified by analysis of chromatin interactions. Nature *485*, 376–380.

Engreitz, J.M., Pandya-Jones, A., McDonel, P., Shishkin, A., Sirokman, K., Surka, C., Kadri, S., Xing, J., Goren, A., Lander, E.S., et al. (2013). The Xist lncRNA exploits three-dimensional genome architecture to spread across the X chromosome. Science *341*, 1237973.

Filion, G.J., van Bemmel, J.G., Braunschweig, U., Talhout, W., Kind, J., Ward, L.D., Brugman, W., de Castro, I.J., Kerkhoven, R.M., Bussemaker, H.J., et al. (2010). Systematic protein location mapping reveals five principal chromatin types in Drosophila cells. Cell *143*, 212–224.

Gallach, M. (2014). Recurrent turnover of chromosome-specific satellites in Drosophila. Genome Biol. Evol. *6*, 1279–1286.

Gilfillan, G.D., Straub, T., de Wit, E., Greil, F., Lamm, R., van Steensel, B., and Becker, P.B. (2006). Chromosome-wide gene-specific targeting of the Drosophila dosage compensation complex. Genes Dev. *20*, 858–870.

Grimaud, C., and Becker, P.B. (2009). The dosage compensation complex shapes the conformation of the X chromosome in Drosophila. Genes Dev. *23*, 2490–2495.

Grimaud, C., and Becker, P.B. (2010). Form and function of dosage-compensated chromosomes–a chicken-and-egg relationship. BioEssays *32*, 709–717.

Heard, E., and Disteche, C.M. (2006). Dosage compensation in mammals: fine-tuning the expression of the X chromosome. Genes Dev. *20*, 1848–1867.

Hou, C., Li, L., Qin, Z.S., and Corces, V.G. (2012). Gene density, transcription, and insulators contribute to the partition of the Drosophila genome into physical domains. Mol. Cell *48*, 471–484.

Ilik, I.A., Quinn, J.J., Georgiev, P., Tavares-Cadete, F., Maticzka, D., Toscano, S., Wan, Y., Spitale, R.C., Luscombe, N., Backofen, R., et al. (2013). Tandem stem-loops in roX RNAs act together to mediate X chromosome dosage compensation in Drosophila. Mol. Cell *51*, 156–173.

Jiang, J., Jing, Y., Cost, G.J., Chiang, J.-C., Kolpa, H.J., Cotton, A.M., Carone, D.M., Carone, B.R., Shivak, D.A., Guschin, D.Y., et al. (2013). Translating dosage compensation to trisomy 21. Nature *500*, 296–300.

Johansson, A.-M., Allgardsson, A., Stenberg, P., and Larsson, J. (2011). msl2 mRNA is bound by free nuclear MSL complex in Drosophila melanogaster. Nucleic Acids Res. *39*, 6428–6439.

Keller, C.I., and Akhtar, A. (2015). The MSL complex: juggling RNA-protein interactions for dosage compensation and beyond. Curr. Opin. Genet. Dev. *31*, 1–11.

Kelley, R.L., Meller, V.H., Gordadze, P.R., Roman, G., Davis, R.L., and Kuroda, M.I. (1999). Epigenetic spreading of the Drosophila dosage compensation complex from roX RNA genes into flanking chromatin. Cell *98*, 513–522.

Kind, J., Vaquerizas, J.M., Gebhardt, P., Gentzel, M., Luscombe, N.M., Bertone, P., and Akhtar, A. (2008). Genome-wide analysis reveals MOF as a key regulator of dosage compensation and gene expression in Drosophila. Cell *133*, 813–828.

Liang, J., Lacroix, L., Gamot, A., Cuddapah, S., Queille, S., Lhoumaud, P., Lepetit, P., Martin, P.G.P., Vogelmann, J., Court, F., et al. (2014). Chromatin immunoprecipitation indirect peaks highlight long-range interactions of insulator proteins and Pol II pausing. Mol. Cell *53*, 672–681.

Lieberman-Aiden, E., van Berkum, N.L., Williams, L., Imakaev, M., Ragoczy, T., Telling, A., Amit, I., Lajoie, B.R., Sabo, P.J., Dorschner, M.O., et al. (2009). Comprehensive mapping of long-range interactions reveals folding principles of the human genome. Science *326*, 289–293.

Magnani, L., Eeckhoute, J., and Lupien, M. (2011). Pioneer factors: directing transcriptional regulators within the chromatin environment. Trends Genet. *27*, 465–474.

Mavrich, T.N., Jiang, C., Ioshikhes, I.P., Li, X., Venters, B.J., Zanton, S.J., Tomsho, L.P., Qi, J., Glaser, R.L., Schuster, S.C., et al. (2008). Nucleosome organization in the Drosophila genome. Nature *453*, 358–362.

Meisel, R.P., and Connallon, T. (2013). The faster-X effect: integrating theory and data. Trends Genet. *29*, 537–544.

Meller, V.H., and Rattner, B.P. (2002). The roX genes encode redundant male-specific lethal transcripts required for targeting of the MSL complex. EMBO J. *21*, 1084–1091.

Nagano, T., Lubling, Y., Stevens, T.J., Schoenfelder, S., Yaffe, E., Dean, W., Laue, E.D., Tanay, A., and Fraser, P. (2013). Single-cell Hi-C reveals cell-to-cell variability in chromosome structure. Nature *502*, 59–64.

Nora, E.P., Lajoie, B.R., Schulz, E.G., Giorgetti, L., Okamoto, I., Servant, N., Piolot, T., van Berkum, N.L., Meisig, J., Sedat, J., et al. (2012). Spatial partitioning of the regulatory landscape of the X-inactivation centre. Nature *485*, 381–385.

Parsch, J., and Ellegren, H. (2013). The evolutionary causes and consequences of sex-biased gene expression. Nat. Rev. Genet. *14*, 83–87.

Quinn, J.J., Ilik, I.A., Qu, K., Georgiev, P., Chu, C., Akhtar, A., and Chang, H.Y. (2014). Revealing long noncoding RNA architecture and functions using domain-specific chromatin isolation by RNA purification. Nat. Biotechnol. *32*, 933–940.

Quinodoz, S., and Guttman, M. (2014). Long noncoding RNAs: an emerging link between gene regulation and nuclear organization. Trends Cell Biol. *24*, 651–663.

Ramírez, F., Dündar, F., Diehl, S., Grüning, B.A., and Manke, T. (2014). deepTools: a flexible platform for exploring deep-sequencing data. Nucleic Acids Res. *42*, W187–W191.

Rao, S.S.P., Huntley, M.H., Durand, N.C., Stamenova, E.K., Bochkov, I.D., Robinson, J.T., Sanborn, A.L., Machol, I., Omer, A.D., Lander, E.S., et al. (2014). A 3D map of the human genome at kilobase resolution reveals principles of chromatin looping. Cell *159*, 1665–1680.

Schneider, I. (1972). Cell lines derived from late embryonic stages of Drosophila melanogaster. J. Embryol. Exp. Morphol. *27*, 353–365.

Sexton, T., Yaffe, E., Kenigsberg, E., Bantignies, F., Leblanc, B., Hoichman, M., Parrinello, H., Tanay, A., and Cavalli, G. (2012). Three-dimensional folding and functional organization principles of the Drosophila genome. Cell *148*, 458–472.

Simon, M.D., Wang, C.I., Kharchenko, P.V., West, J.A., Chapman, B.A., Alekseyenko, A.A., Borowsky, M.L., Kuroda, M.I., and Kingston, R.E. (2011). The genomic binding sites of a noncoding RNA. Proc. Natl. Acad. Sci. USA *108*, 20497–20502.

Simon, M.D., Pinter, S.F., Fang, R., Sarma, K., Rutenberg-Schoenberg, M., Bowman, S.K., Kesner, B.A., Maier, V.K., Kingston, R.E., and Lee, J.T. (2013). High-resolution Xist binding maps reveal two-step spreading during X-chromosome inactivation. Nature *504*, 465–469.

Sofueva, S., Yaffe, E., Chan, W.-C., Georgopoulou, D., Vietri Rudan, M., Mira-Bontenbal, H., Pollard, S.M., Schroth, G.P., Tanay, A., and Hadjur, S. (2013). Cohesin-mediated interactions organize chromosomal domain architecture. EMBO J. *32*, 3119–3129.

Splinter, E., de Wit, E., van de Werken, H.J.G., Klous, P., and de Laat, W. (2012). Determining long-range chromatin interactions for selected genomic sites using 4C-seq technology: from fixation to computation. Methods *58*, 221–230.

Straub, T., Grimaud, C., Gilfillan, G.D., Mitterweger, A., and Becker, P.B. (2008). The chromosomal high-affinity binding sites for the Drosophila dosage compensation complex. PLoS Genet. *4*, e1000302.

Straub, T., Zabel, A., Gilfillan, G.D., Feller, C., and Becker, P.B. (2013). Different chromatin interfaces of the Drosophila dosage compensation complex revealed by high-shear ChIP-seq. Genome Res. *23*, 473–485.

Thomas-Chollier, M., Hufton, A., Heinig, M., O'Keeffe, S., Masri, N.E., Roider, H.G., Manke, T., and Vingron, M. (2011). Transcription factor binding predictions using TRAP for the analysis of ChIP-seq data and regulatory SNPs. Nat. Protoc. *6*, 1860–1869.

Van Bortle, K., Nichols, M.H., Li, L., Ong, C.-T., Takenaka, N., Qin, Z.S., and Corces, V.G. (2014). Insulator function and topological domain border strength scale with architectural protein occupancy. Genome Biol. *15*, R82.

Vaquerizas, J.M., Suyama, R., Kind, J., Miura, K., Luscombe, N.M., and Akhtar, A. (2010). Nuclear pore proteins nup153 and megator define transcriptionally active regions in the Drosophila genome. PLoS Genet. *6*, e1000846.

Vicoso, B., and Charlesworth, B. (2006). Evolution on the X chromosome: unusual patterns and processes. Nat. Rev. Genet. *7*, 645–653.

Zhang, Y., and Oliver, B. (2010). An evolutionary consequence of dosage compensation on Drosophila melanogaster female X-chromatin structure? BMC Genomics *11*, 6.

Zhang, Y., Malone, J.H., Powell, S.K., Periwal, V., Spana, E., Macalpine, D.M., and Oliver, B. (2010). Expression in aneuploid Drosophila S2 cells. PLoS Biol. *8*, e1000320.